

# UC Berkeley

## UC Berkeley Previously Published Works

**Title**

Staging of laser-plasma accelerators

**Permalink**

<https://escholarship.org/uc/item/03h3j1hg>

**Journal**

Physics of Plasmas, 23(5)

**ISSN**

1070-664X

**Authors**

Steinke, S  
van Tilborg, J  
Benedetti, C  
[et al.](#)

**Publication Date**

2016-05-01

**DOI**

10.1063/1.4948280

Peer reviewed

## Staging of laser-plasma accelerators

S. Steinke<sup>\*</sup>, J. van Tilborg, C. Benedetti, C. G. R. Geddes, J. Daniels, K. K. Swanson, A. J. Gonsalves, K. Nakamura, B. H. Shaw, C. B. Schroeder, E. Esarey, and W. P. Leemans

Citation: *Physics of Plasmas* **23**, 056705 (2016); doi: 10.1063/1.4948280

View online: <http://dx.doi.org/10.1063/1.4948280>

View Table of Contents: <http://aip.scitation.org/toc/php/23/5>

Published by the *American Institute of Physics*

---

### Articles you may be interested in

[Enhancement of laser intensity and proton acceleration using micro-tube plasma lens targets](#)

*Physics of Plasmas* **23**, 123122123122 (2016); 10.1063/1.4972577

[Phenomenological theory of laser-plasma interaction in “bubble” regime](#)

*Physics of Plasmas* **11**, (2004); 10.1063/1.1799371


[Energy spread minimization in a cascaded laser wakefield accelerator via velocity bunching](#)

*Physics of Plasmas* **23**, 053106053106 (2016); 10.1063/1.4947536

[Plasma wakefield excitation by incoherent laser pulses: A path towards high-average power laser-plasma accelerators](#)

*Physics of Plasmas* **1777**, 040001040001 (2016); 10.1063/1.4965603

---



Small Conferences. BIG Ideas.

Applied Physics  
Reviews

SAVE THE DATE!  
**3D Bioprinting: Physical and Chemical Processes**  
May 2–3, 2017 • Winston Salem, NC, USA

## Staging of laser-plasma accelerators

S. Steinke,<sup>1,a),b)</sup> J. van Tilborg,<sup>1</sup> C. Benedetti,<sup>1</sup> C. G. R. Geddes,<sup>1</sup> J. Daniels,<sup>1,2</sup>  
 K. K. Swanson,<sup>1,3</sup> A. J. Gonsalves,<sup>1</sup> K. Nakamura,<sup>1</sup> B. H. Shaw,<sup>1,3</sup> C. B. Schroeder,<sup>1</sup>  
 E. Esarey,<sup>1</sup> and W. P. Leemans<sup>1,3</sup>

<sup>1</sup>Lawrence Berkeley National Laboratory, Berkeley, California 94720, USA

<sup>2</sup>Eindhoven University of Technology, PO Box 513, 5600MB Eindhoven, The Netherlands

<sup>3</sup>University of California, Berkeley, California 94720, USA

(Received 15 December 2015; accepted 29 March 2016; published online 2 May 2016)

We present results of an experiment where two laser-plasma-accelerator stages are coupled at a short distance by a plasma mirror. Stable electron beams from the first stage were used to longitudinally probe the dark-current-free, quasi-linear wakefield excited by the laser of the second stage. Changing the arrival time of the electron beam with respect to the second stage laser pulse allowed reconstruction of the temporal wakefield structure, determination of the plasma density, and inference of the length of the electron beam. The first stage electron beam could be focused by an active plasma lens to a spot size smaller than the transverse wake size at the entrance of the second stage. This permitted electron beam trapping, verified by a 100 MeV energy gain. *Published by AIP Publishing.*

[<http://dx.doi.org/10.1063/1.4948280>]

### I. INTRODUCTION

In a laser-plasma accelerator (LPA),<sup>1</sup> an intense, short-pulse laser deposits energy into an underdense plasma via excitation of plasma waves. These plasma waves can provide field gradients exceeding 100 GV/m, enabling extremely compact accelerating structures. The laser energy depletion into plasma waves constitutes a fundamental limitation to particle beam energy gain in an LPA. If particle energies beyond the single stage limit are desired, e.g., for collider-relevant applications,<sup>2,3</sup> operation of LPAs in stages, where each stage is powered by a fresh laser pulse, is required. Obtaining TeV-scale electron beam energies is possible in a single stage; however, this requires operating at low plasma density (on the order of  $\sim 10^{15} \text{ cm}^{-3}$ ), resulting in low accelerating gradients, km-scale acceleration distances, and requires tens of kJ of laser energy. An efficient LPA at such low densities would also require a high bunch charge, increasing beamstrahlung beyond acceptable limits for high-energy physics applications.<sup>4</sup> Hence, LPA staging is critical to the application of LPAs to future colliders. In addition to high-energy physics applications, LPA staging can be important to decelerate electrons after photon production to mitigate shielding needs in compact photon sources.<sup>5</sup>

After the first demonstration of percent-level energy spread and small divergence in mm-scale plasmas in 2004,<sup>6–8</sup> GeV electron beams were obtained with 40 Terawatt (TW) laser pulses,<sup>9</sup> and subsequently, electron beams with multi-GeV energies were reported with Petawatt (PW) class laser systems and few-cm plasmas.<sup>10–12</sup> Controlling the injection of electrons into plasma waves enabled precise tunability of the accelerator.<sup>13–17</sup> Beam emittances of 0.1 mm mrad were reported<sup>18,19</sup> as well as fs bunch durations.<sup>20,21</sup> Such electron

beams represent a suitable source for compact X-ray free-electron lasers<sup>22,23</sup> or Thomson X-ray sources.<sup>24,25</sup>

Here, we present experimental results from a compact, modular staging setup applying two separate laser pulses to drive two independent LPAs.<sup>26</sup> These experiments employed injector electron beams generated from a gas jet target via ionization injection to longitudinally probe the wakefield excited in a second stage target (see Fig. 1(a)). Changing the relative delay of the injector pulse and the second stage laser pulse resulted in a charge modulation of the electron beam that allowed determination of the plasma wavelength  $\lambda_p$  and, hence, the plasma density  $n_e$ . An active plasma lens<sup>27</sup> was introduced to the setup to focus the injector electron beam at the entrance of the second stage target for maximum coupling to the wake (see Fig. 1(b)). Numerical modeling was compared against experimental measurements to infer the temporal structure and to investigate the influence of the transverse plasma profile in the second stage.

### II. EXPERIMENT CONFIGURATION

To establish a stable injector stage, 70% of the BELLA center TREX 40 TW laser pulse (i.e., 1.3 J laser energy, 45 fs duration) was focused by a 2 m focal length parabola down to a beam waist of  $w_0 = 18 \mu\text{m}$  onto a supersonic deLaval gas jet of 700  $\mu\text{m}$  diameter. A mixture of two gases (99% helium and 1% nitrogen) was used to increase the amount of trapped charge. Injection was achieved by ionizing deeply bound electrons from the high atomic number gas (nitrogen) around the peak of the laser pulse, i.e., at a phase inside the wakefield that allows them to be trapped.<sup>28,29</sup>

Stable electron beams were routinely produced over hours of run time (corresponding to thousands of laser shots and more than 10 days). By changing the distance of the laser focus and the gas jet nozzle, the beam parameters could be tuned in energy and charge. For the two experiments presented in this paper (Sections II and III), this injector was

Note: Paper T13 6, Bull. Am. Phys. Soc. 60, 306 (2015).

<sup>a)</sup>Invited speaker.

<sup>b)</sup>ssteinke@lbl.gov

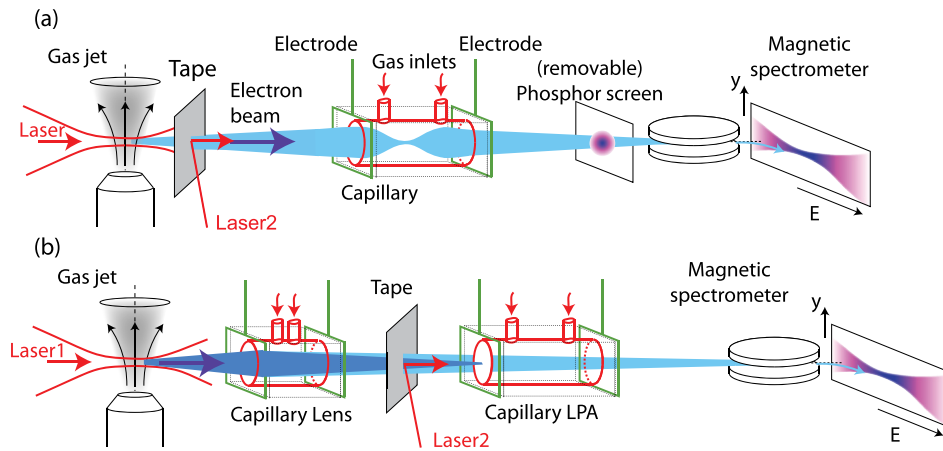


FIG. 1. Experimental setup. (a) In stage I, a laser pulse is focused on a gas jet, producing the injector electron beam. In stage II, the beam enters a discharge capillary. A second laser pulse modulates the electrons; this laser is coupled to the second discharge capillary via a plasma-mirror tape. A magnetic spectrometer is used to obtain an energy-dispersed electron profile. This setup was used for the experiments discussed in Section III. (b) An additional discharge capillary is introduced in the setup, acting as a plasma lens to refocus the electron beam to the entrance of stage II. This setup was used for the experiments discussed in Section IV.

adjusted to generate beams with two different sets of parameters. For the experiments in Section II [III], beam with mean energies of  $(72 \pm 3)$  [ $(120 \pm 5)$ ] MeV, 85% [60%] (FWHM) energy spread, beam charge of  $(19 \pm 2)$  [ $(33 \pm 5)$ ] pC, and low divergence  $(5 \pm 0.3)$  [ $(4 \pm 0.3)$ ] mrad were obtained with a pointing stability of 0.3 mrad (standard deviation). The energy spread of 85% for the experiments of Section II corresponds to an upper limit estimate as it was taken from the lower end (40 MeV) of a blind region of the electron spectrometer (between 40 MeV and 50 MeV).

A capillary discharge waveguide structure was used as a second stage LPA target (see Fig. 1). The discharge current creates a preformed plasma that serves as a waveguide, guiding the driving laser pulse over many Rayleigh lengths, minimizing diffraction and extending the acceleration length. These target systems are well characterized,<sup>9,30</sup> and a model has previously been developed permitting the determination of the wakefield amplitude and the on-axis density by means of the spectral redshift of the transmitted laser.<sup>10,31</sup> A feedback-controlled, tape-based plasma-mirror system (PM) was used to combine the injector beam with the laser driver for the second stage. The PM has a laser energy throughput of 80%, insignificant laser mode or pointing degradations, and has been fully characterized and developed to provide uninterrupted operation at a repetition rate of 1 Hz for hours of run time.<sup>32</sup>

The second stage laser pulse (450 mJ energy, 45 fs duration) was applied to drive a wakefield in the discharge capillary as described in Ref. 31. Matched propagation of a transversely Gaussian laser pulse in a plasma with a transverse parabolic density profile of the form  $n = n_0 + \alpha r^2$  can be obtained, at low laser power and intensity, if the input laser spot size,  $w_0$ , equals the matched spot size,  $r_m$  [for a parabolic plasma profile, the matched spot size is given by  $r_m = (\alpha \pi r_e)^{-1/4}$ , with  $r_e = 2.8 \times 10^{-13}$  cm being the classical electron radius, and  $\alpha$  being the channel depth parameter]. Our experimental conditions lead to mismatched propagation and, hence, to varying peak intensities and wakefield strengths along the waveguide (see discussion

below). Wake excitation under these conditions was confirmed by measuring optical spectra of the transmitted laser pulse. Analysis of the spectra revealed a maximum relative redshift of 3% with respect to the central wavelength of the laser at a density of  $2 \times 10^{18} \text{ cm}^{-3}$ . This corresponds to an average field amplitude of 17 MV/mm if wake excitation occurs over the full length of the capillary.<sup>31</sup>

### III. DIRECT LONGITUDINAL WAKEFIELD PROBING AND INFERENCE OF THE ELECTRON BUNCH LENGTH

In the experimental configuration without the plasma lens, corresponding to Fig. 1(a), the delay of the two laser pulses was varied by an optical delay stage in the laser beam line of the injector stage. Electron spectra were recorded as a function of the delay between the two laser pulses driving the first- and the second stage (see Fig. 2).

In the case of a positive delay, the first stage electrons propagated only under the influence of the discharge magnetic field without the impact of the second laser pulse. After the second laser pulse arrived (negative delay), the electron spectra were periodically modulated in energy and charge (Fig. 2(a)). The bandwidth of the modulation is illustrated by means of electron spectra at the extrema in Fig. 2(b). Where, at the delay for maximum charge throughput, 50% of the input charge distribution reached the magnetic spectrometer, almost no charge is transmitted 60 fs later. In Fig. 2(c), the integrated charge is plotted showing the persistence of the modulation for delays corresponding to more than 10 plasma wave periods. In Fig. 2(d), the Fast Fourier Transform (FFT) of the charge modulation is shown, verifying the constant period of the modulation of  $18 \mu\text{m}$ . This is consistent with a plasma frequency  $\omega_p$  at a density of  $3.4 \times 10^{18} \text{ cm}^{-3}$ .

Accompanying numerical modeling with the code INF&RNO<sup>33,34</sup> allows interpretation of the experimental findings. A laser pulse similar to the experiment with an energy of 360 mJ was modeled with a Gaussian shape in time with a duration of 45 fs (FWHM) and an Airy profile in

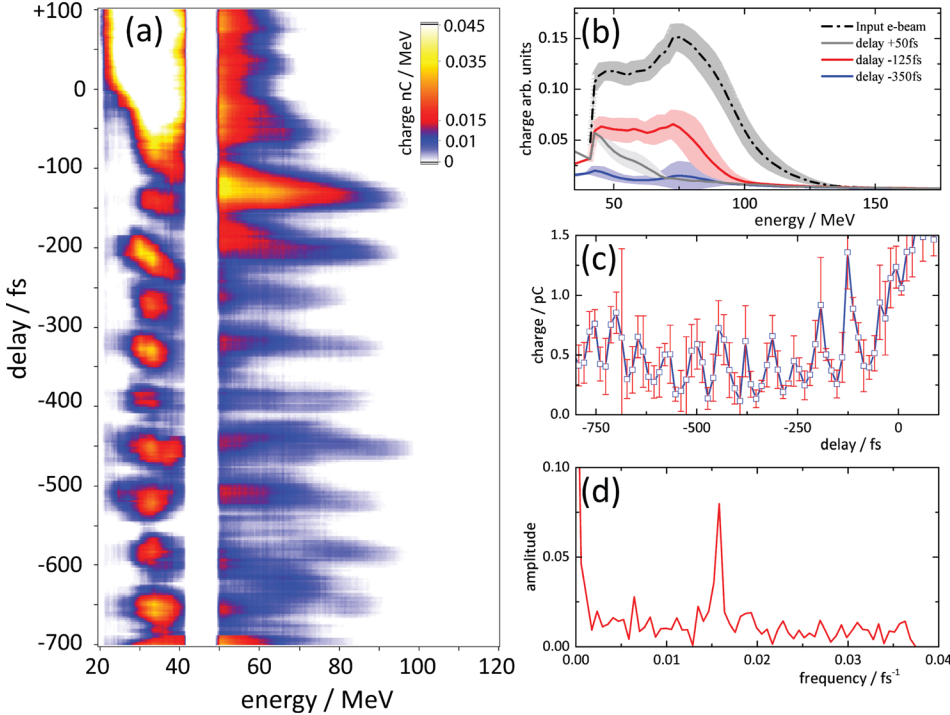


FIG. 2. (a) Injector electron beams probing the wakefield of the 2nd stage: waterfall plot of normalized electron spectra shown horizontally in color code. Each row represents a 5-shot averaged spectrum. Positive delay: The injector electrons arrive before the 2nd stage laser pulse and propagate unaffected by the laser. Negative delay: The 1st stage electrons are influenced by the presence of the wakefield generated by the 2nd stage laser pulse. (b) Averaged electron spectra (5 shots) for three different delays (see plot legend for details) plotted along with in the input spectrum. (c) Integrated electron beam charge as a function of the delay of the electron beam with respect to the wake-driving laser pulse. (d) FFT of (c).

space. The plasma density profile in the capillary of 33 mm length was linearly increasing for 3 mm (to account for the gas supply slots in the experiment) followed by a plateau region of 27 mm length with a density of  $3.4 \times 10^{18} \text{ cm}^{-3}$  and a linearly decreasing ramp for another 3 mm. The focal plane of the laser was located at the beginning of the density plateau. A radially varying external magnetic field  $B(r) = \mu_0 I_0 r / (2\pi R^2)$  was applied, for a discharge current of 325 A to account for the electron beam focusing.

To obtain more information on the temporal structure of the input electron bunch, the delay scan was repeated with different bunch lengths (see Fig. 3). The distinct charge/energy modulation obtained with short initial bunches became indistinct if the bunch length exceeds  $\lambda_p/2$ , as expected. Best agreement with the experimental values is achieved at a bunch length of  $\leq 5 \mu\text{m}$  (see Fig. 3).

When the laser is present, the transverse force of the laser-induced wake prevents a complete focusing of the electron bunch. The waist of the electron bunch is smaller than the

transverse size of the wake only in the region where the laser is defocused due to mismatched guiding, and hence, the longitudinal wakefield is small. This results in a relatively small energy gain/loss of the electron beam of  $\pm 25 \text{ MeV}$ . However, when the transversal size of the wake is small, i.e., the field amplitude is high, most electrons are deflected since they experience defocusing fields due to their oblique incidence as they approach the wake. As a result, only a very small fraction of the electrons experience an appreciable accelerating wake.

#### IV. MULTISTAGE COUPLING OF INDEPENDENT LPAs

In order to efficiently trap the electron beam in the second stage wakefield, an active plasma lens<sup>27</sup> was inserted after the gas jet (see Fig. 1(b)). The relative phasing of the electron beam and the second stage laser was controlled by the delay of the two driving laser pulses, and electron spectra were again recorded for each delay. Similar to the case without the plasma lens, the electron spectra were periodically

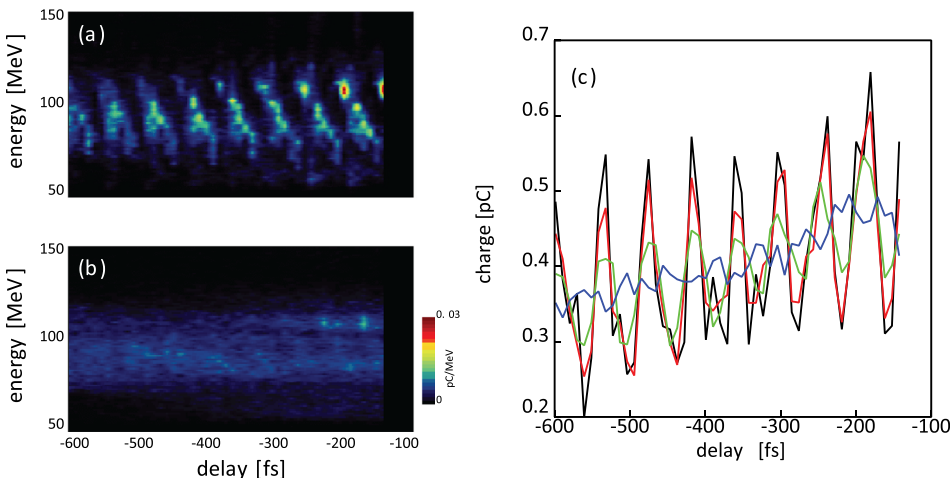


FIG. 3. Electron spectra as a function of the delay between the arrival of the electron bunch and laser pulse driving the wake for different electron bunch lengths: (a)  $2.5 \mu\text{m}$  and (b)  $20 \mu\text{m}$ . The electron bunch charge for different initial bunch lengths as a function of the delay between electron bunch and laser:  $2.5 \mu\text{m}$  (black),  $5 \mu\text{m}$  (red),  $10 \mu\text{m}$  (green), and  $20 \mu\text{m}$  (blue). Only electrons within a full divergence of 5 mrad were taken into account.

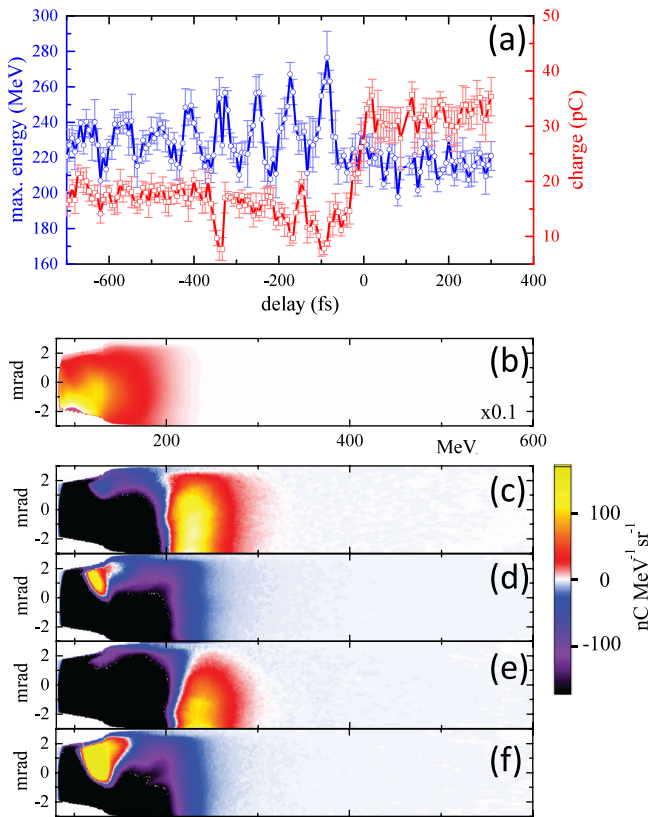


FIG. 4. Spectra of electron beams from staged acceleration:<sup>26</sup> (a) maximum electron energy (blue) and total electron beam charge (red) as a function of the delay of the two driving laser pulses. A single data point represents an average of 5 measurements, and the error bar is the standard deviation. (b) 100-shot average unperturbed reference for delays of 100–300 fs before arrival of the second laser pulse. (c)–(f) 2D charge maps (5-shot average) subtracted by the reference (b) for the first two maxima and minima of the energy oscillation shown in (a), i.e., for delays of  $-107$  fs,  $-153$  fs,  $-193$  fs, and  $-240$  fs, respectively. Reproduced with permission from Steinke *et al.*, Nature **530**, 190 (2016). Copyright 2016 Nature.<sup>26</sup>

modulated in energy (Fig. 4(a)). The period of the modulation was  $(80 \pm 6)$  fs, consistent with a plasma wavelength  $\lambda_p = 24 \mu\text{m}$  at a density of  $(1.9 \pm 0.3) \times 10^{18} \text{cm}^{-3}$ . The constant periodicity of the observed modulation as a

function of the delay behind the driver pulse further indicates a quasi-linear wake, consistent with expectations for the experimental parameters including laser intensity and plasma density.

To investigate the influence of the second stage wakefield on the electron beam in detail, a reference spectrum of an unperturbed beam (positive delay) was subtracted from the spectrum at each delay to emphasize the effect while maintaining absolute charge information. The resulting electron distributions are plotted in Fig. 5(a) and the simulation results in Fig. 5(b) in the form of a waterfall plot of electron spectra, where each horizontal line corresponds to a 5-shot averaged energy spectrum. Background-subtracted 2D charge maps, also averaged over 5 shots, are shown in Figs. 4(c)–4(f) for significant delays. The presence of the second-stage laser results in a reduction of total beam charge of up to a factor of 3 (see Fig. 4(a)). For appropriate timing of the second stage laser, however, charge was detected beyond the energy cut-off of the input electron spectrum, i.e.,  $>200$  MeV. This charge accelerated beyond the cutoff of the input spectrum, shown by the red and yellow areas in Figs. 4(c) and 4(e), indicates acceleration in the second stage. The integrated charge in this region of  $1.2$  pC represents the charge trapped in the accelerating phase of the wake and, respectively, a trapping efficiency of 3.5%. At delays of  $\lambda_p/2$  after the times of maximum energy gain,  $\sim 1$  pC of additional charge was detected around  $110$ – $150$  MeV (Figs. 4(d) and 4(f)). This could correspond to electrons decelerated or to electrons deflected by the transverse wake fields into the spectrometer acceptance. The broad energy spread of the first stage electron beam prevents unambiguous observation of the decelerating phase of the wake under these conditions.

As discussed above, there were two regions of increased laser intensity, and hence higher wake amplitude, in the capillary due to mismatched laser pulse guiding. In Fig. 6, the electron energy evolution is plotted as a function of propagation in the capillary for two different electron populations. One population of electrons focused by the active plasma lens to a spot size  $<15 \mu\text{m}$  had an initial energy in the interval

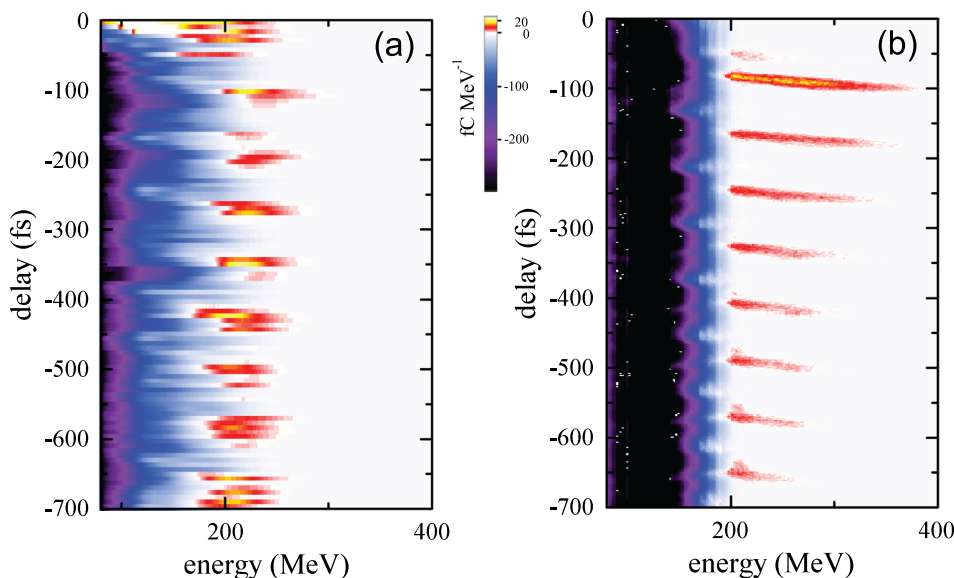


FIG. 5. Waterfall plot of electron spectra as function of delay:<sup>26</sup> (a) experimental data (each spectrum is a 5-shot average) and (b) simulation results. Each spectrum was subtracted by the reference (positive delay). Reproduced with permission from Steinke *et al.*, Nature **530**, 190 (2016). Copyright 2016 Nature.<sup>26</sup>

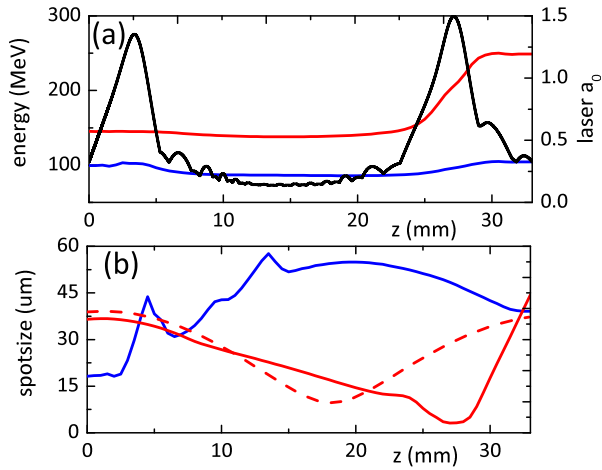


FIG. 6. (a) Evolution of the laser intensity expressed as the normalized laser vector potential  $a_0$  (black) and evolution of electron energy as function of propagation in the capillary for two different electron populations: electrons with an initial energy in the interval 89–130 MeV at a delay of  $-304$  fs (blue) and electrons with a final energy of 200–300 MeV at a delay of  $-252$  fs (red). (b) Evolution of the electron beam rms spot size for the same electron beam subsets as in (a) and the electron beam rms spot size of the electrons with final energy 200–300 MeV without the influence of the laser field. Reproduced with permission from Steinke *et al.*, Nature **530**, 190 (2016). Copyright 2016 Nature.<sup>26</sup>

89–130 MeV at a delay of  $-304$  fs, gained 95 MeV of energy in the region  $z = 2$ –5 mm, but were strongly defocused by the transverse wakefield in  $z = 5$ –8 mm.

The population of electrons with a final energy above 200 MeV experienced a 100 MeV energy gain at a delay of  $-252$  fs in the vicinity of the 2nd laser focus, corresponding to a propagation distance of  $z = 24$ –29 mm in the plasma, where, due to the focusing induced by the discharge current and the laser-induced wake, they reach a spot-size of  $5 \mu\text{m}$  and interact strongly with the laser-driven plasma wake. This is shown Fig. 6(b), where we plot (red solid line) the evolution of the transverse electron bunch size as a function of the propagation distance. The red dashed line in the same figure shows the evolution of the bunch spot size without the influence of the laser pulse, indicating that the contribution of the external magnetic field induced by the discharge current of the second capillary on the trapping of the electrons cannot be neglected.

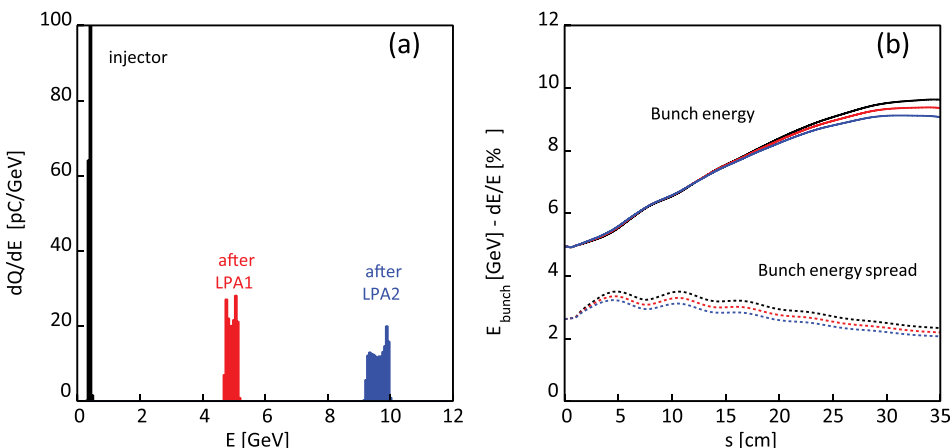


FIG. 7. (a) Electron spectra at different stages of the simulation. (b) Mean electron energy and relative energy spread as a function of propagation in the second stage capillary for 3 different timings:  $-434.6$  fs (black),  $-430.8$  fs (red), and  $-426.9$  fs (blue).

## V. STAGING SCALING TOWARDS PW-CLASS LASER

For energy gains of multiple GeV per stage, as required for collider applications,<sup>2,3</sup> lasers with PW power such as BELLA<sup>35</sup> are required. In order to model such a multi-GeV staging prototype, we adapted the setup sketched in Fig. 1(b) for two identical Gaussian (temporally and spatially) laser drivers, with 15 J pulse energy, 80 fs (FWHM) pulse duration, and  $w_0 = 53 \mu\text{m}$  beam waist. An electron beam with beam parameter similar to the one obtained in Ref. 13 with a central energy of 400 MeV, 4% energy spread and 10 pC charge were accelerated in the first LPA stage (LPA1): a discharge capillary of 30 cm length and a parabolic channel with a matched radius of  $70 \mu\text{m}$  and a plasma density of  $2.2 \times 10^{17} \text{cm}^{-3}$ . The injector beam is trapped completely and accelerated to energies of 4.5 GeV at an energy spread of 2.5% and 0.11 mrad divergence, consistent with the experimental results reported in Ref. 10. A 9 cm long active plasma lens<sup>27</sup> with a radius of  $250 \mu\text{m}$  and a current of 800 A is applied to provide the focusing fields required to couple the electron beam to the second stage (LPA2, identical to LPA1) at a total coupling distance of 40 cm. The second stage laser pulse is introduced by PM situated 20 cm upstream of LPA2. For proper timing of the two laser pulses, the first stage electron beam can be trapped entirely in the quasi-linear wakefield excited by the second laser pulse and accelerated to energies of 9.5 GeV while maintaining low relative energy spread and divergence. In Fig. 7(b), energy spread and bunch energy are plotted for 3 different timings to demonstrate the robustness with respect to jitter in the system.

## VI. CONCLUSION

In summary, we have presented an experimental study of staging of two LPAs independently driven by two synchronized laser pulses. Electron beam injection and capture into the second stage wake were demonstrated by means of an  $\sim 100$  MeV energy gain recurring at delays corresponding to multiples of  $\lambda_p$ . The observation of temporally well-defined energy modulations further directly implies a bunch length of the input electron beam shorter than  $\lambda_p/4$ . This experimental result represents a major milestone in the development of laser-driven plasma-based accelerators towards future colliders, as well as other LPA application that

requires electron energies beyond the single stage limits and/or that requires deceleration of electrons after use to mitigate shielding requirements. Numerical modeling indicates that multi-GeV energy boosts to high quality electron beams (with 100% trapping) can be achieved by operating at lower densities (i.e., larger transverse wake size).

## ACKNOWLEDGMENTS

The authors thank N. H. Matlis, S. Shiraishi, and T. Sokollik for their contributions to the initial construction of the setup and an early version of the experiment, as well as C. Toth, D. Syversrud, N. Ybarrolaza, M. Kirkpatrick, G. Mannino, T. Sipla, D. Evans, R. Duarte, D. Baum, D. Munson for their contributions. This work was supported by the U.S. Department of Energy Office of Science Office of High Energy Physics, under Contract No. DE-AC02-05CH11231, by the U.S. Department of Energy National Nuclear Security Administration, Defense Nuclear Nonproliferation R&D (NA22) and by the National Science Foundation (NSF) under Contract Nos. 0917687 and 0935197. This research used computational resources (Edison, Hopper) of the National Energy Research Scientific Computing center (NERSC), which is supported by the Office of Science of the U.S. Department of Energy under Contract No. DE-AC02-05CH11231.

- <sup>1</sup>E. Esarey, C. B. Schroeder, and W. P. Leemans, *Rev. Mod. Phys.* **81**, 1229 (2009).
- <sup>2</sup>W. P. Leemans and E. Esarey, *Phys. Today* **62**(3), 44 (2009).
- <sup>3</sup>C. B. Schroeder, E. Esarey, C. G. R. Geddes, C. Benedetti, and W. P. Leemans, *Phys. Rev. Spec. Top.—Accel. Beams* **13**, 101301 (2010).
- <sup>4</sup>C. B. Schroeder, E. Esarey, and W. P. Leemans, *Phys. Rev. Spec. Top.—Accel. Beams* **15**, 051301 (2012).
- <sup>5</sup>S. G. Rykovanov, C. G. R. Geddes, J. L. Vay, C. B. Schroeder, E. Esarey, and W. P. Leemans, *J. Phys. B: At. Mol. Opt. Phys.* **47**, 234013 (2014).
- <sup>6</sup>C. G. R. Geddes, C. Toth, J. van Tilborg, E. Esarey, C. B. Schroeder, D. Bruhwiler, C. Nieter, J. Cary, and W. P. Leemans, *Nature* **431**, 538 (2004).
- <sup>7</sup>S. P. D. Mangles, C. D. Murphy, Z. Najmudin, A. G. R. Thomas, J. L. Collier, A. E. Dangor, E. J. Divall, P. S. Foster, J. G. Gallacher, C. J. Hooker *et al.*, *Nature* **431**, 535 (2004).
- <sup>8</sup>J. Faure, Y. Glinec, A. Pukhov, S. Kiselev, S. Gordienko, E. Lefebvre, J. P. Rousseau, F. Burgy, and V. Malka, *Nature* **431**, 541 (2004).
- <sup>9</sup>W. P. Leemans, B. Nagler, A. J. Gonsalves, C. Toth, K. Nakamura, C. G. R. Geddes, E. Esarey, C. B. Schroeder, and S. M. Hooker, *Nat. Phys.* **2**, 696 (2006).
- <sup>10</sup>W. P. Leemans, A. J. Gonsalves, H. S. Mao, K. Nakamura, C. Benedetti, C. B. Schroeder, C. Tóth, J. Daniels, D. E. Mittelberger, S. S. Bulanov *et al.*, *Phys. Rev. Lett.* **113**, 245002 (2014).
- <sup>11</sup>X. M. Wang, R. Zgadzaj, N. Fazel, Z. Y. Li, S. A. Yi, X. Zhang, W. Henderson, Y. Y. Chang, R. Korzekwa, H. E. Tsai *et al.*, *Nat. Commun.* **4**, 1988 (2013).
- <sup>12</sup>H. T. Kim, K. H. Pae, H. J. Cha, I. J. Kim, T. J. Yu, J. H. Sung, S. K. Lee, T. M. Jeong, and J. Lee, *Phys. Rev. Lett.* **111**, 165002 (2013).
- <sup>13</sup>A. J. Gonsalves, K. Nakamura, C. Lin, D. Panasenkov, S. Shiraishi, T. Sokollik, C. Benedetti, C. B. Schroeder, C. G. R. Geddes, J. van Tilborg *et al.*, *Nat. Phys.* **7**, 862 (2011).
- <sup>14</sup>J. Faure, C. Rechatin, A. Norlin, A. Lifschitz, Y. Glinec, and V. Malka, *Nature* **444**, 737 (2006).
- <sup>15</sup>J. S. Liu, C. Q. Xia, W. T. Wang, H. Y. Lu, C. Wang, A. H. Deng, W. T. Li, H. Zhang, X. Y. Liang, Y. X. Leng *et al.*, *Phys. Rev. Lett.* **107**, 035001 (2011).
- <sup>16</sup>V. Malka, A. Lifschitz, J. Faure, and Y. Glinec, *Phys. Rev. Spec. Top.—Accel. Beams* **9**, 091301 (2006).
- <sup>17</sup>A. Lifschitz, J. Faure, Y. Glinec, V. Malka, and P. Mora, *Laser Part. Beams* **24**, 255 (2006).
- <sup>18</sup>G. R. Plateau, C. G. R. Geddes, D. B. Thorn, M. Chen, C. Benedetti, E. Esarey, A. J. Gonsalves, N. H. Matlis, K. Nakamura, C. B. Schroeder *et al.*, *Phys. Rev. Lett.* **109**, 064802 (2012).
- <sup>19</sup>M. Schnell, A. Sävert, B. Landgraf, M. Reuter, M. Nicolai, O. Jäckel, C. Peth, T. Thiele, O. Jansen, A. Pukhov *et al.*, *Phys. Rev. Lett.* **108**, 075001 (2012).
- <sup>20</sup>O. Lundh, J. Lim, C. Rechatin, L. Ammoura, A. Ben-Ismaïl, X. Davoine, G. Gallot, J. P. Goddet, E. Lefebvre, V. Malka *et al.*, *Nat. Phys.* **7**, 219 (2011).
- <sup>21</sup>A. Buck, M. Nicolai, K. Schmid, C. M. S. Sears, A. Savert, J. M. Mikhailova, F. Krausz, M. C. Kaluza, and L. Veisz, *Nat. Phys.* **7**, 543 (2011).
- <sup>22</sup>Z. R. Huang, Y. T. Ding, and C. B. Schroeder, *Phys. Rev. Lett.* **109**, 204801 (2012).
- <sup>23</sup>A. R. Maier, A. Meseck, S. Reiche, C. B. Schroeder, T. Seggebrock, and F. Grüner, *Phys. Rev. X* **2**, 031019 (2012).
- <sup>24</sup>C. G. R. Geddes, S. Rykovanov, N. H. Matlis, S. Steinke, J.-L. Vay, E. H. Esarey, B. Ludewigt, K. Nakamura, B. J. Quiter, C. B. Schroeder *et al.*, *Nucl. Instrum. Methods Phys. Res. Sect. B* **350**, 116 (2015).
- <sup>25</sup>N. D. Powers, I. Ghebregziabher, G. Golovin, C. Liu, S. Chen, S. Banerjee, J. Zhang, and D. P. Umstadter, *Nat. Photonics* **8**, 29 (2014).
- <sup>26</sup>S. Steinke, J. van Tilborg, C. Benedetti, C. G. R. Geddes, C. B. Schroeder, J. Daniels, K. K. Swanson, A. J. Gonsalves, K. Nakamura, N. H. Matlis *et al.*, *Nature* **530**, 190 (2016).
- <sup>27</sup>J. van Tilborg, S. Steinke, C. G. R. Geddes, N. H. Matlis, B. H. Shaw, A. J. Gonsalves, J. V. Huijts, K. Nakamura, J. Daniels, C. B. Schroeder *et al.*, *Phys. Rev. Lett.* **115**, 184802 (2015).
- <sup>28</sup>A. Pak, K. A. Marsh, S. F. Martins, W. Lu, W. B. Mori, and C. Joshi, *Phys. Rev. Lett.* **104**, 025003 (2010).
- <sup>29</sup>C. McGuffey, A. G. R. Thomas, W. Schumaker, T. Matsuoka, V. Chvykov, F. J. Dollar, G. Kalintchenko, V. Yanovsky, A. Maksimchuk, K. Krushelnick *et al.*, *Phys. Rev. Lett.* **104**, 025004 (2010).
- <sup>30</sup>D. J. Spence and S. M. Hooker, *Phys. Rev. E* **63**, 015401 (2000).
- <sup>31</sup>S. Shiraishi, C. Benedetti, A. J. Gonsalves, K. Nakamura, B. H. Shaw, T. Sokollik, J. van Tilborg, C. G. R. Geddes, C. B. Schroeder, C. Toth *et al.*, *Phys. Plasmas* **20**, 063103 (2013).
- <sup>32</sup>T. Sokollik, S. Shiraishi, J. Osterhoff, E. Evans, A. J. Gonsalves, K. Nakamura, J. van Tilborg, C. Lin, C. Toth, and W. P. Leemans, *AIP Conf. Proc.* **1299**, 233 (2010).
- <sup>33</sup>C. Benedetti, C. B. Schroeder, E. Esarey, and W. P. Leemans, in *Proceedings of ICAP2012, Rostock-Warnemünde, Germany, 2012* (JACoW, Geneva, 2012), p. THAAI2.
- <sup>34</sup>C. Benedetti, C. B. Schroeder, E. Esarey, C. G. R. Geddes, and W. P. Leemans, *AIP Conf. Proc.* **1299**, 250 (2010).
- <sup>35</sup>W. P. Leemans, J. Daniels, A. Deshmukh, A. J. Gonsalves, A. Magana, H. S. Mao, D. E. Mittelberger, K. Nakamura, J. R. Riley, D. Syversrud *et al.*, in *Proceedings of 2013 Particle Accelerator Conference* (2013), p. THYAA1.